Research Article

# High-Fidelity Photovoltaic Emulation Using an ANFIS Model and Advanced Control Strategies

*Abdelkarim CHOHRA*[1], *Khaled AMEUR*[1], *Aboubakeur HADJAISSA*[1,*], *Nabil ABOUCHABANA*[1], *Mohammed BENMILOUD*[1], *Abdelhamid RABHI*[2]

[1]LACoSERE laboratory, Amar Telidji University of Laghouat, Laghouat, Algeria
[2] MIS laboratory, Jules Verne University of Picardy, Amiens, France

aek.chohra@lagh-univ.dz, b.hadjaissa@lagh-univ.dz, kh.ameur@lagh-univ.dz, n.abouchabana@lagh-univ.dz, med.benmiloud@lagh-univ.dz , abdelhamid.rabhi@u-picardie.fr

[*]Corresponding author: Aboubakeur HADJAISSA; b.hadjaissa@lagh-univ.dz

DOI: 10.15598/aeee.v24ix.251009

Article history: Received Oct 09, 2025; Revised Feb 04, 2026; Accepted Apr 10, 2026; Published Dec xx, 202x.


***Abstract.*** *This study introduces an advanced photovoltaic (PV) emulator designed to precisely mimic the electrical characteristics of PV panels under dynamic environmental and load conditions. This study proposes a photovoltaic emulator that combines an Adaptive Neuro-Fuzzy Inference System (ANFIS)–based PV model with several control strategies, including PI, Fuzzy Logic Control (FLC), and Model-Free Control (MFC), in a unified evaluation framework. The proposed PV emulator integrates three key elements: a high-accuracy ANFIS model that robustly captures the nonlinear current-voltage (I–V) and power-voltage (P–V) characteristics of PV panel, serving as a dynamic reference; a DC-DC buck converter as the power stage; and a control framework that comparatively evaluates proportional-integral (PI), Fuzzy Logic Control (FLC), and the proposed MFC method. Among the controllers, the Model-Free Control (MFC) approach is particularly effective owing to its adaptability and robustness, operating without reliance on a precise system model while effectively managing uncertainties and non-linearities. Simulation results across diverse irradiance, temperature, and load scenarios confirm that the MFC-based emulator, combined with the ANFIS reference, achieves superior tracking accuracy, faster dynamic response, and improved stability, outperforming the PI and FLC controllers in terms of lower steady-state error, reduced overshoot, and shorter settling times. This emulator provides a reliable, cost-effective, and safe platform for testing MPPT algorithms, power converters, and grid-connected renewable energy systems, thereby supporting the rapid advancement and deployment of solar energy technology.*

## Keywords

***PV Emulator (PVE), ANFIS Model, DC-DC Buck Converter, Proportional-Integral (PI), Fuzzy Logic, Model-Free Control (MFC)***

## 1. Introduction

The global transition to sustainable energy, propelled by the imperatives of climate change mitigation and energy security, has established renewable sources as central to future infrastructure [1, 2]. Among these, solar photovoltaic (PV) energy is a pivotal technology that harnesses the most abundant and widely distributed energy resource on Earth—sunlight. Solar PV offers a clean, silent, and scalable solution, with installations ranging from residential rooftops to utility-scale solar farms, and has experienced exponential growth driven by dramatic cost reductions and sustained-policy support. Its modular nature and ability to generate electricity directly from light make it uniquely suited for diverse applications, from grid support to powering remote communities [3]. However, the inherent characteristics of solar energy and its dependence on intermittent meteorological conditions pose significant challenges for technology development. The electrical output of a PV module is a complex nonlinear function of solar irradiance, cell temperature, and load conditions. This variability makes the controlled laboratory testing of solar-dependent hardware, such as inverters, charge controllers, and energy management systems, difficult and unreliable when actual solar panels are used [4]. This critical gap in the research and development workflow underscores the necessity of the photovoltaic emulator (PVE). A PVE is a sophisticated programmable power supply that accurately mimics the current-voltage (I-V) and power-voltage (P-V) characteristics of real PV arrays under any simulated environmental or electrical scenario. By providing a stable, repeatable, and weather-independent "virtual sun," it enables rigorous, year-round testing and optimization of solar power electronics [5].

The PV emulator thus serves as an indispensable bridge between solar energy's real-world potential and the reliable engineering required to harness it. It decouples innovation from environmental constraints, accelerating the development cycle, reducing costs, and ensuring the robustness of solar energy systems before field deployment [6, 7]. The current status of PVE research is hindered by two primary issues: the difficulty in solving the nonlinear static and dynamic equations of PV cells/modules and the challenge of efficient PVE control [8].

Research on photovoltaic emulators often focuses on three fundamental parts: photovoltaic models [9],control strategies [10], and power converters [11]. The following sections provide a brief overview of contemporary advancements in each element.

- **Photovoltaic Models:** The literature outlines two main considerations regarding the photovoltaic model used for the photovoltaic emulator. The first pertains to the types of photovoltaic models, which can be classified into two categories: the electrical circuit model, [12, 13] and the interpolation model, as shown in Figure 1 [9].The second aspect concerns the implementation methods for the PV model in the emulator's controller. Standard methods include the look-up table approach [14], piecewise linear method [15], neural network method [16, 17], and photovoltaic voltage elimination method [18], as shown in Figure 2.

- **Control Strategy:** The control strategy of PV emulators, including traditional and advanced control methods, has emerged as an essential subject in photovoltaics within the PVE domain. The control strategy for the PVE system aims to achieve the operational point defined by the photovoltaic model (current/voltage) by minimizing the error between the measured value and the reference value defined by the PV model.

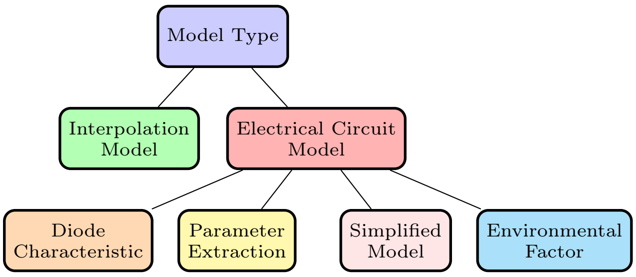


**Fig. 1:** PV Model Type

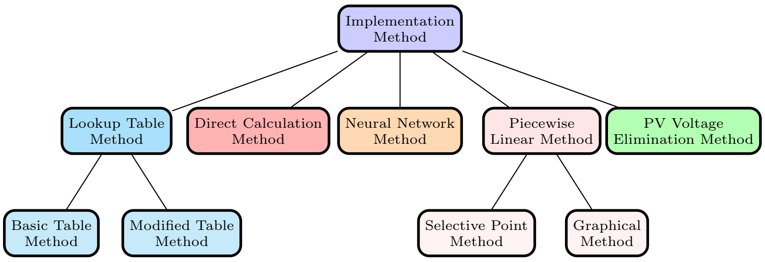


**Fig. 2:** Implementation Method of PV models

This method accurately reproduces the output impedance of a photovoltaic panel. Several approaches have been proposed in the literature to improve the efficiency, reliability, and robustness of PVE systems under diverse operating conditions, considering environmental fluctuations and working conditions, [19]. Here are a few strategies that utilize known controllers, including fractional PID (Proportional-Integral-Derivative) [20], PI (Proportional-Integral) Controller [21], LQR (Linear Quadratic Regulator) [17], Fuzzy Logic [22, 23], Fuzzy PID Controller [24], SMC (Sliding Mode Control) [8, 25], and MFC (Model-Free Control) [26], MPC (Model Predictive Control) [27].

- **Power Converter:** Different types of power converters are used in PV emulators to supply power to loads. These converters can be classified into three main categories: linear regulators, switched-mode power supplies (SMPS), and programmable power supplies (PPS). Switched-mode power supplies (SMPS) are the most commonly used type of converter, and they stand out from other types because of several advantages. These include higher efficiency, compact size, lighter weight, wide input voltage range, reduced heat generation, excellent voltage regulation, scalability, higher power density, and greater ease in controlling the output voltage and current [11].

  This classification includes non-isolated converters, such as boost, buck, Cuk, zeta, and SEPIC converters [28], as well as isolated converters, including flyback, forward,bridge, multiport, and push-pull converters [29].

This study presents the design and validation of an advanced, high-fidelity photovoltaic (PV) emulator. The proposed system integrates three core components: 1) an Adaptive Neuro-Fuzzy Inference System (ANFIS) for real-time PV model computation, 2) a DC-DC buck converter as the power stage, and 3) an advanced control layer implemented and compared across three distinct strategies: Proportional-Integral (PI) control, Fuzzy Logic Control (FLC), and Model-Free Control (MFC).

The main contribution of this work is not limited to the use of ANFIS within a photovoltaic emulator, but rather lies in a set of technical enhancements that address specific limitations observed in existing ANFIS-based PVE implementations. In particular, the proposed approach introduces the following key novelties and distinguishing aspects:

- ANFIS-based approaches have been investigated in the literature for modeling nonlinear PV characteristics. In this work, ANFIS is employed as the reference model within a PV emulator framework, which enables accurate reproduction of the I–V characteristics under varying environmental conditions.

- The proposed approach introduces a model-free control (MFC) strategy for PV emulation. Unlike conventional PI and fuzzy logic controllers, the MFC does not rely on an explicit model of the buck converter. It is based on an ultra-local model updated online from input–output measurements, allowing improved robustness to nonlinearities, parameter uncertainties, and load variations.

- A unified evaluation framework is adopted in which PI, fuzzy logic, and model-free controllers are tested using the same PV–ANFIS model and the same buck converter. This configuration enables a fair comparison of tracking performance, robustness to load disturbances, and implementation complexity under identical operating conditions.

In summary, the proposed emulator is validated through simulations under varying irradiance, temperature, and load conditions. The results demonstrate that integrating the dynamic PV-ANFIS model with the advanced MFC strategy achieves high tracking accuracy and robustness. Collectively, these contributions establish a flexible, high-fidelity PV emulation framework, providing a critical tool for the design, testing, and validation of advanced solar energy systems.

## 2. Proposed PV Emulator

Figure 3 illustrates the structure of the proposed emulator, which consists of three main parts:

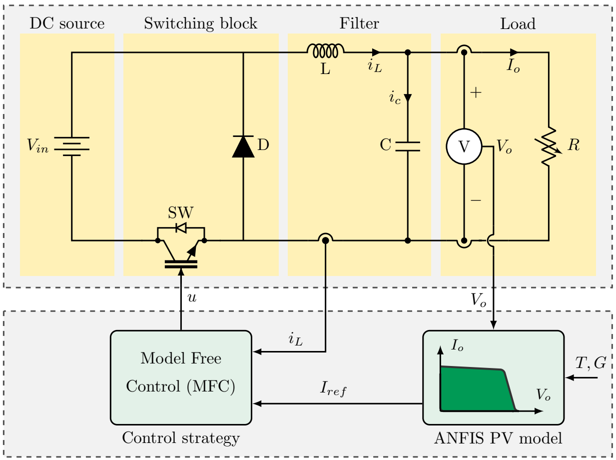


**Fig. 3:** Block diagram of the proposed PV emulator

- **Power Converter:** The power converter employed in this paper is a DC-DC buck converter. It is controlled using a current-mode strategy to track the reference point generated by the PV-ANFIS model.

- **Control Strategy:** This ensures that the output current of the buck converter follows its reference exactly as determined by the PV-ANFIS model.

- **PV-ANFIS Model:** The PV-ANFIS model generates the reference current based on the measured voltage of the buck converter, irradiance, and temperature. After being trained using the generated dataset from PV electrical model.

### 2.1. DC-DC Buck Converter: Description and Modelling

Figure 4.(a) depicts the electrical circuit of the buck converter supplied by a DC source. It consists of two switches, an inductor, and a capacitor, and supplies a resistive load.

The switching function of the system, denoted as $u$, defines two operating modes [30]:

- **Mode 1 (Charging Mode):** When $u = 1$, switch $S$ is activated while $D$ is off, Figure4.(b) .

- **Mode 2 (Discharging Mode):** When $u = 0$, switch $S$ is deactivated while $D$ is on, Figure4.(c) .

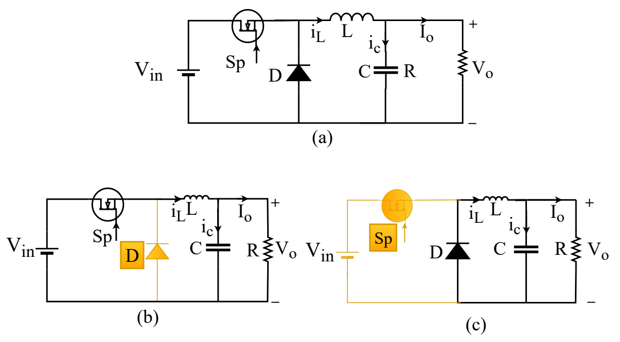


**Fig. 4:** Circuit diagram of a buck converter

The capacitor voltage ($V_c$) and inductor current ($i_L$) serve as state variables. Two active control modes are defined by $u$, and the buck converter model is determined by (1) and (2).

$$L\frac{di_L}{dt} = V_{in}u - V_c \tag{1}$$

$$C\frac{dV_c}{dt} = i_c - \frac{V_c}{R} \tag{2}$$

This model can be rewritten in the following state-space representation by (3) and (4), [31].

$$\dot{x} = Ax + Bu \tag{3}$$

$$y = Cx + Du \tag{4}$$

where:

$$A = \begin{bmatrix} 0 & -\frac{1}{L} \\ \frac{1}{C} & -\frac{1}{RC} \end{bmatrix} \quad B = \begin{bmatrix} \frac{V_{in}}{L} \\ 0 \end{bmatrix}, \quad C = \begin{bmatrix} 1 & 0 \end{bmatrix}$$

Based on the state-space representation for Mode 1 (Switch ON) and Mode 2 (Switch OFF), the transfer function is derived using equation (1) and (2)

$$G(s) = C(sI - A)^{-1}B \tag{5}$$

After determining the switching frequency (fs), the maximum allowable current ripple for the inductor $\Delta i_{L\max}$ should be established as follows: The minimum value of the inductor $L_{\min}$ can then be calculated using the equation provided in Eq.(6).

$$L_{\min} = \frac{V_{\text{in}}}{4 \times f_s \times \Delta i_{L_{\max}}} \tag{6}$$

where $\Delta i_{L_{\max}}$ denotes the current ripple. The role of the capacitor is to reduce the voltage ripples, which is determined by Eq.(7).

$$C = \frac{\Delta i_{L_{\max}}}{8 \times f_s \times \Delta V_{o_{\max}}} \tag{7}$$

where $\Delta V_{o_{\max}}$ is the output voltage ripple [6,31].

## 2.2. Control Strategy: Analysis and Design

In this work, three controllers were studied, PI, FLC and MFC, for controlling PVE, with the objective of selecting the most suitable one based on dynamic performance criteria: response time and steady-state error.

### 1) Proportional-Integral controller (PI)

The standard proportional-integral (PI) controller is widely used owing to its simplicity and ease of practical implementation [32]. However, its main limitation is the tuning of the its gains, as the robustness may degrade under rapid variations in irradiance, temperature, or load. For the DC-DC buck converter that controller generating the required duty cycle $D$ as PWM signal [21,33].

Furthermore, the designs of both the PI controller and buck converter adhered to the principles established in [34].

The transfer function of the buck converter, eq.(8), and the PI controller , eq.(9), are given by [30,31,34].

$$G_s(s) = \frac{I(s)}{d(s)} = \frac{V_{\text{in}}(RCs + 1)}{RCLs^2 + Ls + R} \tag{8}$$

$$G_c(s) = \frac{U}{E} = \frac{K_p s + K_i}{s} \tag{9}$$

The closed-loop transfer function is obtained from the following expression [35].

$$H(s) = \frac{G_s.G_c}{1 + G_s.G_c} \tag{10}$$

$$H(s) = \frac{V_{\text{in}}(RCs + 1)(K_p s + K_i)}{s(RCLs^2 + Ls + R) + V_{\text{in}}(RCs + 1)(K_p s + K_i)} \tag{11}$$

The values of the proportional gain $Kp$ and integral gain $Ki$ are determined using the well-known Ziegler-Nichols tuning method, as summarized in Table 1, [36]

**Tab. 1:** PI controller parameters.

| Parameter | Value |
|---|---|
| $K_p$ | $9.98 \times 10^0$ |
| $K_i$ | $1.50 \times 10^0$ |

### 2) Fuzzy Logic Controller

The fuzzy logic controller is one of the most effective and robust control techniques, requiring no system modelling. It offers robust control without relying on traditional design methods, such as root locus, frequency response, or pole placement techniques. The fuzzy logic controller functions through three key processes: fuzzification, fuzzy inference, and defuzzification. [37, 38]. However, its performance strongly depends on the choice of membership functions and rule base, making the tuning time-consuming and highly designer-dependent. Moreover, it offers limited formal guarantees of stability/robustness and may require higher computational effort than a PI controller, particularly under rapid changes in irradiance, temperature, or load. The FLC controller was designed with two inputs: the error $e(t)$ and and its derivative (change of error) $\Delta e(t)$. These inputs are defined as:

$$e(t) = I_{\text{ref}}(t) - I(t), \tag{12}$$

$$\Delta e(t) = \frac{de(t)}{dt} \approx \frac{e(t) - e(t-1)}{\Delta t}, \tag{13}$$

where $I_{\text{ref}}(t)$ is the reference current generated by PV-ANFIS model and $I(t)$ is the measured current. The fuzzy inference process maps these inputs to a single control action, defined as the pulse-width modulation (PWM) duty cycle $D \in [0, 1]$.

- For the first input there are seven membership functions: Negative Big (NB), Negative Medium (NM), Negative Small (NS), Zero (ZE), Positive Small (PS), Positive Medium (PM), and Positive Big (PB).
- The second input, characterized by seven membership functions: Negative Big (NB), Negative Medium (NM), Negative Small (NS), zero (ZE), Positive Small (PS), Positive Medium (PM), and Positive Big (PB).
- The output of the FLC controller, also characterized by seven membership functions: Negative Big (NB), Negative Medium (NM), Negative Small (NS), Zero (ZE), Positive Small (PS), Positive Medium (PM), and Positive Big (PB).

**Tab. 2:** Fuzzy rule base.

| $\Delta E$ \ $E$ | **NB** | **NM** | **NS** | **ZE** | **PS** | **PM** | **PB** |
|---|---|---|---|---|---|---|---|
| **NB** | NB | NB | NB | NB | NM | NS | ZE |
| **NM** | NB | NB | NB | NM | NS | ZE | PS |
| **NS** | NB | NB | NM | NS | ZE | PS | PM |
| **ZE** | NB | NM | NS | ZE | PS | PM | PB |
| **PS** | NM | NS | ZE | PS | PM | PB | PB |
| **PM** | NS | ZE | PS | PM | PB | PB | PB |
| **PB** | ZE | PS | PM | PB | PB | PB | PB |

The fuzzy inference process combines the membership functions with control rules to generate a fuzzy output. This process involves logical operations and transforms inputs to outputs using "If-Then" rules, known as fuzzy rules, which are detailed in Table 2. The defuzzification stage, which is performed using the centroid method, provides a precise output value for the fuzzy logic control system [38].

### 3) Model-Free Control (MFC)

Compared with the PI and Fuzzy Logic controllers described previously, the Model-Free Control (MFC) strategy is presented in a detailed manner as it constitutes the main control approach investigated in this study. The PI and FLC controllers are well-established techniques and are primarily included as benchmark methods to enable a fair performance comparison with the proposed MFC-based PV emulator.

Model-Free Control (MFC) is a modern and effective control technique that eliminates the need for precise mathematical modeling of complex systems or systems with uncertainty. Unlike traditional model-based methods, which depend on comprehensive and accurate descriptions of system dynamics, the MFC directly estimates system behavior using real-time input-output data. This approach is particularly effective for dealing with nonlinearities and disturbances [39]. The fundamental principle of the MFC approach is to replace the unknown system dynamics with an ultra-local model, which is typically expressed as:

$$y^{(n)} = F + \beta u \tag{14}$$

Where $\beta \in \mathbb{R}$ is a *non-physical*, chosen such that $F$ and $\beta u$ are of the same magnitude. The numerical value of $F$, which encapsulates the system's structural information, is determined based on the knowledge of $u$, $\beta$, and the estimated derivative $y^{(n)}$, as described in [40].

***Selection of Parameter $\beta$:*** The parameter $\beta$ plays a crucial role in the MFC structure, scaling the control input to match the order of magnitude of the system dynamics. In this study, $\beta$ was empirically tuned through a systematic procedure to ensure optimal performance:

1. **Initial Estimation**: A standard test was conducted by introducing step changes in irradiance (from 400 to 1000 $W/m^2$) and temperature (from 25°C to 55°C) while observing the output current and voltage of the PV emulator.
2. **Performance Metrics**: The system's response was evaluated using key performance indices:
   - Overshoot (%)

- Settling time (s)
- Root Mean Square Error (RMSE)
- Integral of Absolute Error (IAE)

3. **Iterative Tuning**: The value of $\beta$ was varied over a range (e.g., $10^3$ to $10^5$), and the above metrics were recorded for each $\beta$.

   The chosen value $\beta = 10{,}000$ minimizes the RMSE and IAE while maintaining an acceptable overshoot and settling time, as validated in Scenario 2 ( Table 6).

4. **Validation Under Dynamic Conditions**: The selected $\beta$ was further validated under varying loads and environmental conditions (Scenarios 3 and 4), confirming its robustness across different operating points.

***MFC Implementation:*** The MFC controller was implemented in a progressive and structured manner.

1. **Ultra-Local Model Construction**: The first-order ultra-local model ($n = 1$) was used:

$$\dot{y} = F + \beta u \tag{15}$$

2. **Real-Time Estimation of** $F$: At each sampling instant $k$, $F_{k-1}$ is estimated from past input–output data using:

$$F_{k-1} = \dot{y}_{k-1} - \beta u_{k-1} \tag{16}$$

   where $\dot{y}_{k-1}$ is obtained via the noise-robust numerical differentiation method given in Eq. (18).

3. **Control Law Computation**: The control input $u_k$ is computed as:

$$u_k = -\frac{1}{\beta}\left(F_{k-1} - \dot{y}^*_k\right) + C(y^*_k - y_k) \tag{17}$$

   where:

   - $y^*$ is the reference current generated by the ANFIS model,
   - $C$ is a PI corrector with $K_p = 1.6$, $K_i = 0$ (proportional only in this implementation),
   - $\beta = 10{,}000$.

4. **Noise-Robust Differentiation**: To compute $\dot{y}$ from noisy measurements, the following finite-time integration formula was applied over a sliding window $[0, T]$:

$$\hat{\dot{y}} = -\frac{3!}{T^3}\int_0^T (T - 2t)y(t)\,dt \tag{18}$$

   with $T = 0.001$ s in this study.

5. **Discretization and Real-Time Execution**: The control algorithm was implemented in MATLAB/Simulink with a fixed-step solver (ode1 Euler) and a sampling time of $1 \times 10^{-5}$ s to match the switching frequency of 20 kHz.

6. **MFC Parameter Summary** :

   - $\beta = 10{,}000$
   - $T$ (differentiation window) $= 0.001$ s
   - $K_p = 1.6$, $K_i = 0$
   - Sampling time $T_s = 1 \times 10^{-5}$ s
   - Buck converter parameters: as per Table 5

These implementation details, along with the provided parameter values and tuning methodology, ensure that the MFC-based PV emulator can be accurately reconstructed and validated in similar experimental and simulation environments.

## 2.3. PV-ANFIS Model

### 1) Electrical Model of PV Panel

The PV panel model is a crucial component of photovoltaic energy systems. Therefore, the emulated panel model must be precise before the PVE can be evaluated in the model. Numerous solar panel models have been proposed in the literature [6, 11].In this study, we employed a widely used one-diode model to represent the PV panels, as shown in Figure 5. This model provides an excellent balance between simplicity and accuracy, making it a popular choice among power electronic designers for simulating PV systems [6, 41]. Specifically, a PV panel block was used with SOLARWORLD SW 85 poly R5A/D.

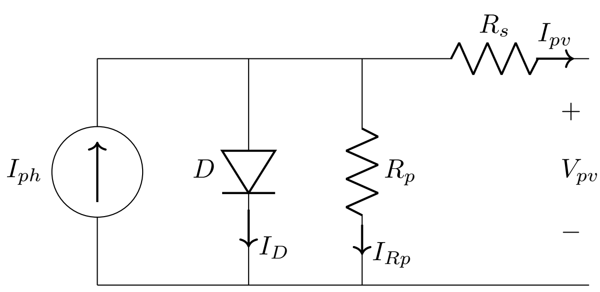


**Fig. 5:** PV module equivalent single-diode (1D2R) circuit .

$$I_{pv} = I_{ph} - I_o\left[\exp\left(\frac{V_{pv} + R_s I_{pv}}{V_t A}\right) - 1\right] - \frac{V_{pv} + R_s I_{pv}}{R_p} \tag{19}$$

with:

- $I_{ph}$: Photoelectric current (A)

- $I_o$ : Diode saturation current (A)
- $V_t$ : Junction thermal voltage (V)
- $V_{pv}$ : Terminal voltage (V)
- $R_s$ :Cell series resistance ($\Omega$)
- $R_p$ : Cell shunt resistance ($\Omega$)
- A : Diode ideality factor

The PV panel characteristics of the proposed model are presented in Table 3.

**Tab. 3:** PV panel characteristics.

| | |
|---|---|
| **Rated max. power** $P_{\max}$ | 85 W |
| **Open-circuit voltage** $V_{\mathrm{oc}}$ | 22 V |
| **Rated voltage** $V_{\mathrm{mpp}}$ | 17.9 V |
| **Short-circuit current** $I_{\mathrm{sc}}$ | 5.20 A |
| **Rated current** $I_{\mathrm{mpp}}$ | 4.77 A |
| **Temp. coeff. of** $V_{\mathrm{oc}}$ | $-0.37\,\%/\mathrm{K}$ |
| **Temp. coeff. of** $I_{\mathrm{sc}}$ | $0.081\,\%/\mathrm{K}$ |

### 2) ANFIS Architecture

Developed in the 1990s as part of the Soft Computing paradigm, it combines the human-like ability to reason and learn under uncertain and imprecise conditions. It operates as an adaptive network that is structurally equivalent to a fuzzy inference system, allowing for the direct implementation of the Sugeno model. The Adaptive Neuro-Fuzzy Inference System (ANFIS) has gained considerable attention owing to its hybrid intelligence and versatile modelling capabilities. By integrating neural networks with the learning and modelling strengths of fuzzy inference systems (FIS), ANFIS creates an adaptive inference system, [42, 43].

Recently, hybridisation trends have combined data-driven intelligence (ANFIS) with robust or predictive control to enhance transient performance and robustness. Predictive current control implemented with ANFIS on a dSPACE platform has been demonstrated for power electronic converters, highlighting the feasibility of integrating ANFIS with predictive control frameworks (MPC-type) in real-time [44]. Moreover, sliding-mode control remains a common robust option in PV power conversion under fast environmental variations, motivating hybrid ANFIS–SMC structures to mitigate uncertainties while preserving a strong dynamic response [45].

As show the figure 6, a dataset was generated from a photovoltaic panel ( Figure 5) and subsequently used to train an Adaptive Neuro-Fuzzy Inference System (ANFIS) with three inputs: irradiance, temperature, and mesured voltage. The current refernce served as the output for the ANFIS model in this study. This

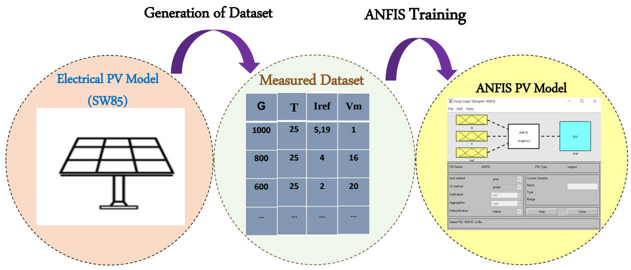


**Fig. 6:** Training process of the PV-ANFIS

method effectively captures the nonlinear relationships between environmental parameters and photovoltaic panel performance, facilitating enhanced optimization.

### 3) Training of ANFIS

For the training step of ANFIS, the Sugeno method was used, which includes three inputs: irradiance, temperature, and voltage. The output of this model was the current reference. Current-voltage (I-V) data were used for both the training and testing of the model. The ANFIS constructs a fuzzy inference system (FIS) in which the parameters of the membership functions are optimized using a hybrid training approach. This method combines least-squares estimation techniques with the backpropagation algorithm.

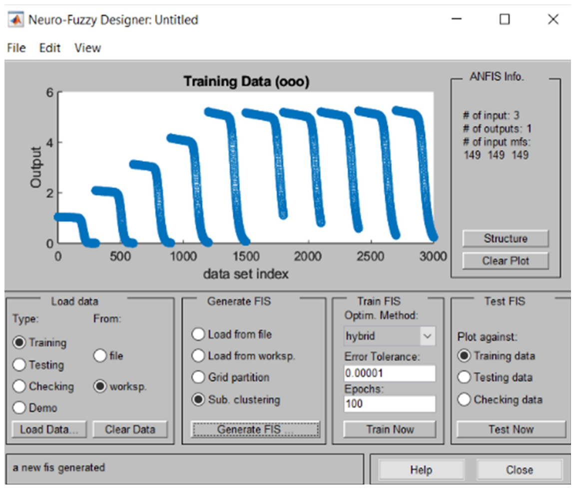


**Fig. 7:** PV dataset based PV electrical model

Figure 7 illustrates the load of the PV dataset generated from the electrical model in Simulink Matlab in the ANFIS environment. The training process used the parameters outlined in Table 4 to ensure that the model accurately represented the nonlinear relationship between the current and voltage under varying load conditions and environmental changes, as shown in Figure 8. After training, the resulting ANFIS PV model was evaluated using the loaded dataset to assess its effectiveness and reliability,as shown in Figure 9.

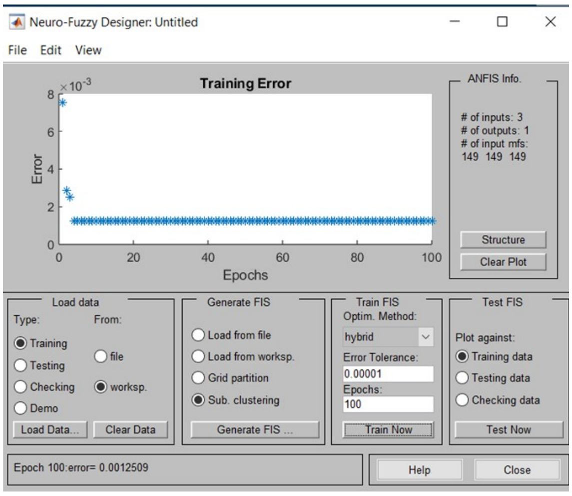


**Fig. 8:** ANFIS training data

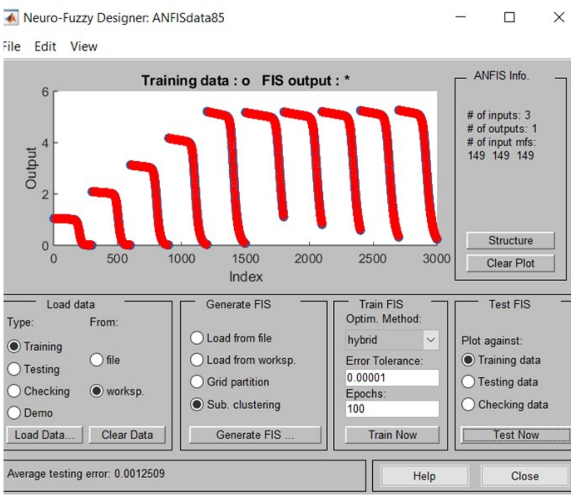


**Fig. 9:** Tested data

The Adaptive Neuro-Fuzzy Inference System (ANFIS) constructs a fuzzy inference system (FIS) in which the parameters of the membership functions are optimized using a hybrid training approach. This method combines least-squares estimation techniques with the backpropagation algorithm to ensure that the model accurately represents the nonlinear relationship between the current and voltage under varying load conditions and environmental changes. After training, the resulting ANFIS PV model was evaluated using the loaded dataset to assess its effectiveness and reliability [43].

Figure 10 shows the rule structure of the PV-ANFIS model, demonstrating the relationships between the inputs, membership functions, rules, and outputs. The input membership functions (MFs) are shown in figure 11 for the voltage input variable, and Figure 12 displays the MFs for the output variable ( reference current).

**Tab. 4:** ANFIS training parameters.

| Parameter | Definition / Values |
|---|---|
| Membership functions | 149 |
| Optimisation method | Hybrid |
| Error tolerance | 0.0012509 |
| Epochs | 100 |

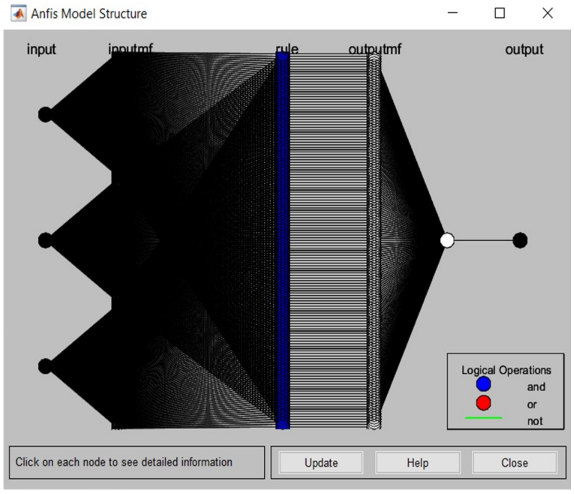


**Fig. 10:** ANFIS model structure

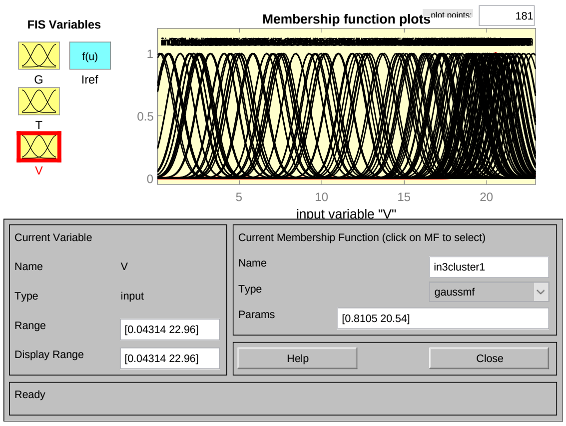


**Fig. 11:** Membership functions of voltage

## 4) Validation of the ANFIS PV Model

To demonstrate the performance of the ANFIS PV model, a test was conducted comparing it with the PV panel model (SW85) under standard test conditions (STC).

Figures 13 and 14 present the I–V and P–V characteristics of the SW85 photovoltaic panel under different environmental conditions .This further demonstrates the strong agreement between the electrical model (SW85) and the ANFIS-based PV model. Specifically, Figure 13 confirms this consistency across irradiance levels ranging from 200 W/m$^2$ to 1000 W/m$^2$ at a fixed temperature of 25 C°, whereas Figure 14 illustrates the comparison over temperatures varying from 5 C°

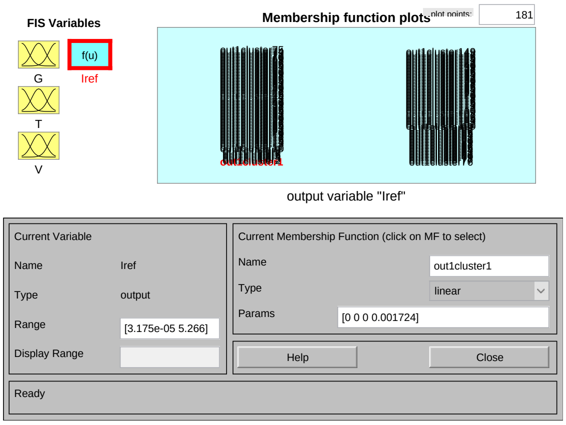


**Fig. 12:** Membership functions of reference Current

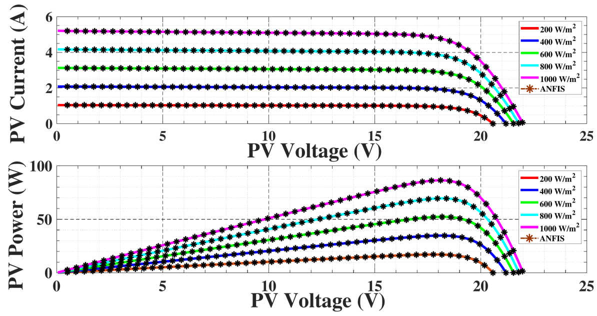


**Fig. 13:** PV panel vs PV-ANFIS model: validation of I-V and P-V curves at varying irradiance levels (T = 25°C)

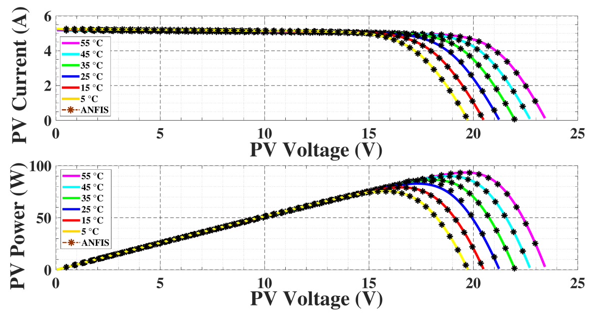


**Fig. 14:** PV panel vs PV-ANFIS model: validation of I-V and P-V curves at varying temperature values (Irr=1000 W/m²)

to 55 C° under a constant irradiance of 1000 W/m². These results validate the ability of the ANFIS model to accurately emulate the nonlinear behavior of the PV panel under both irradiance and temperature variations, thereby confirming its robustness and reliability for dynamic PV emulation.

**Remark:** Despite the relatively large number of membership functions (149), the ANFIS model demonstrates strong generalization capability. This is ensured by the hybrid training approach, which optimizes both premise and consequent parameters, and by validating the model on a separate dataset not used during training. As shown in Figures 9, 13, and 14, the model accurately reproduces the I–V and P–V characteristics of the PV panel across a wide range of irradiance and temperature conditions, confirming that it reliably predicts PV behavior under varying operating scenarios without overfitting.

# 3. Results and discussion

To evaluate the proposed PV emulator (Figure 3), which integrates the PV-ANFIS model with a buck converter, PI controller, FLC controller, and MFC Controller, we conducted a comparative analysis. This analysis involved simulating and testing the MFC, FLC, and conventional PI controllers under varying load, irradiance, and temperature conditions.

The buck converter parameters used in these calculations are listed in Table 5.

**Tab. 5:** Component values of the buck converter.

| **Parameter** | **Value** |
|---|---|
| Input voltage, $V_{\text{in}}$ | 40 V |
| Switching frequency, $f$ | 20 kHz |
| Output resistance, $R_o$ | $1\,\Omega$–$20\,\Omega$ |
| Output voltage ripple factor, $r_{vo}$ | 2% |
| Current ripple factor (CRF) | 14.3% |
| Inductor, $L$ | 0.724 mH |
| Capacitor, $C$ | 23.6 $\mu$F |

To achieve this, four scenarios were selected. The main objective of these scenarios was to evaluate and compare the performance of three candidate controllers—Proportional-Integral (PI), Fuzzy Logic Control (FLC), and Model-Free Control (MFC)—in governing a photovoltaic (PV) emulator, each scenario designed to rigorously assess the adaptability, robustness, and accuracy of the emulator under controlled conditions mimicking real-world PV operation.

The comparative analysis across these scenarios serves as the basis for selecting the most effective control strategy.

## 3.1. Scenario 1

In scenario 1, the load resistance was initially set to 3.75 Ω, at which the panel operated at its maximum power point (MPP). It was then reduced to 2 Ω, increased to 5.5 Ω, and finally returned to 3.75 Ω, all under conditions of 1000 W/m² and 25 °C, as shown in Figure 15.

From Figure 16, it can be observed that the MFC achieved a lower error and reduced ripple compared with the PI and FLC, demonstrating superior precision and robustness in PV emulation. Figures 17 and

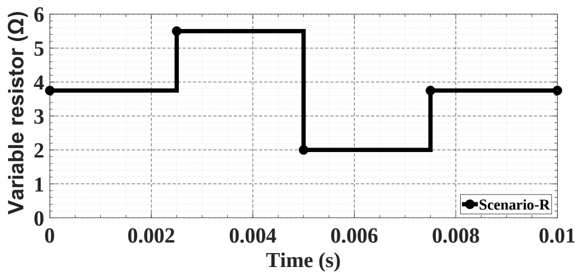


**Fig. 15:** Scenario 1: load variation at STC

18 provide further comparisons of voltage and power, where the MFC controller outperforms the others in terms of better tracking and stability.

To quantitatively confirm this superiority, four performance indices were evaluated: Root Mean Square Error (**RMSE**), integral square error (**IAE**), **settling time**, and **overshoot** which are reported in Table 6 to better illustrate the performance enhancement of the proposed controller.

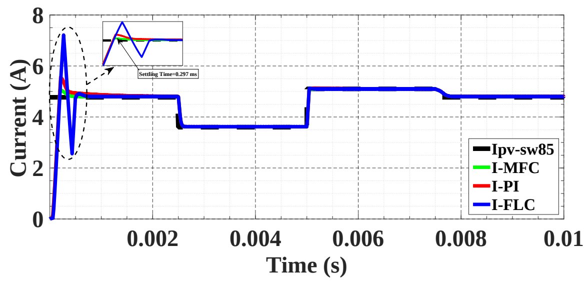


**Fig. 16:** PV emulator current response under varying load resistances

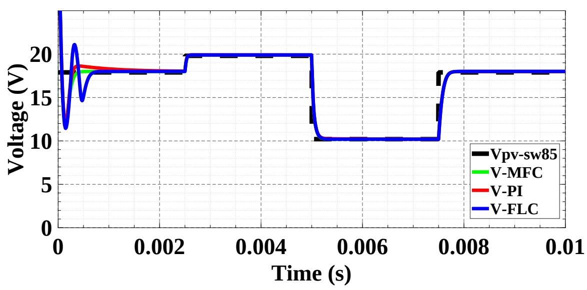


**Fig. 17:** PV emulator voltage response under varying Load resistances

**Tab. 6:** Comparison of SW85 panel with MFC, FLC, and PI currents based PVE at a load resistance (3.75 Ω).

| Control strategy | Overshoot (%) | IAE | Settling time (s) | RMSE |
|---|---|---|---|---|
| MFC | 6.7460 | 5.5281e−4 | 2.9732e−4 | 0.2637 |
| FLC | 47.0142 | 7.2746e−4 | 3.2465e−4 | 0.3156 |
| PI | 14.3577 | 6.8962e−4 | 5.0490e−4 | 0.2739 |

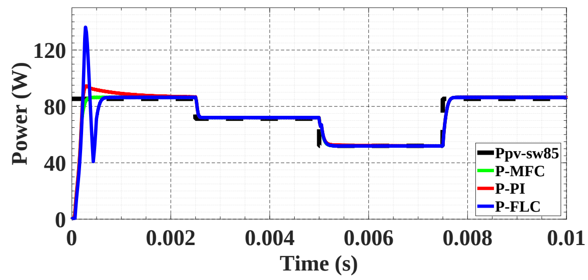


**Fig. 18:** PV emulator power response under varying load resistances

## 3.2. Scenario 2

In Scenario 2, to illustrate the efficacy of our PVE under irradiance change, as shown in Figure 19, the PV electrical model SW85 served as a reference for the proposed PVE regulated by the MFC, FLC, and PI while maintaining a constant load and temperature. In this scenario, the load was established at 3.75 Ω and the temperature was fixed at 25 C°. The irradiance varied from 400 W/m$^2$ to 600 W/m$^2$ between 0 and 0.002 s, thereafter increasing from 580 W/m$^2$ to 1000 W/m$^2$ between 0.004 and 0.006 s,and finally decreasing from 1000 W/m$^2$ to 800 W/m$^2$ over 582 the time frame from 0.008 to 0.01 s.

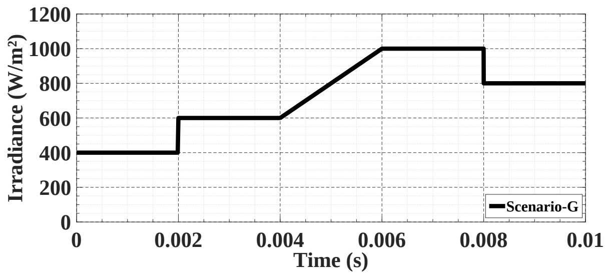


**Fig. 19:** Scenario 2: Solar irradiance variation

Based on the analysis presented in Figure 20, it can be concluded that the behavior of the ANFIS-based PV emulator closely aligned with that of the reference electrical PV model SW85 when subjected to sudden variations in irradiance. This comparison confirmed the effectiveness of the proposed PV-ANFIS model. Furthermore, the current regulation is illustrated, and the results summarized in Table 7 highlight the superior performance of the MFC compared to the PI and FLC controllers. Figures 21 and 22 validate the PVE performance. These figures illustrate how the output voltage and power adjust in response to variations in irradiance, showcasing the system's capability to maintain stable voltage and power despite changing environmental conditions.

Together, these highlight the robustness of the PVE and underscore the effectiveness of the MFC controller in delivering reliable performance under dynamic variations in irradiance.

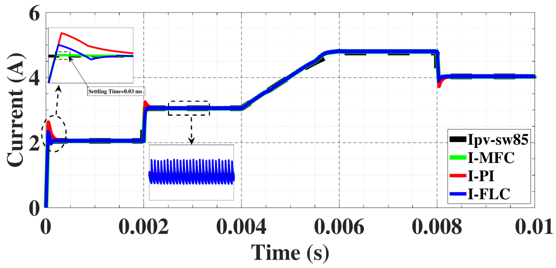


**Fig. 20:** PV emulator current response under irradiance variations

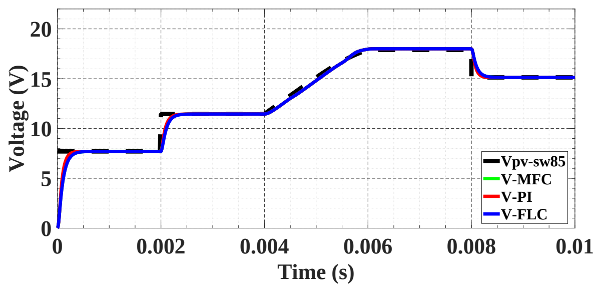


**Fig. 21:** PV emulator voltage response under irradiance variations

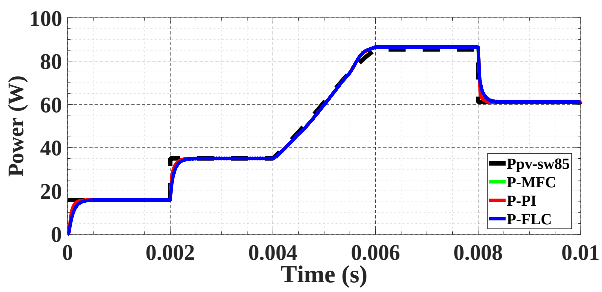


**Fig. 22:** PV emulator power response under irradiance variations

**Tab. 7:** Comparison of SW85 current with MFC, FLC and PI currents at 400 W/m$^2$ irradiance.

| Control strategy | Overshoot (%) | IAE | Settling time (s) | RMSE |
|---|---|---|---|---|
| MFC | 1.4869 | 1.9670e−4 | 3.6990e−5 | 0.0728 |
| FLC | 37.6795 | 1.8095e−4 | 2.4053e−4 | 0.0948 |
| PI | 28.1078 | 8.8653e−5 | 2.1821e−4 | 0.0812 |

## 3.3. Scenario 3

In Scenario 3, as shown in Figure 23, the temperature changes from 25 C° to 55 C° between 0 and 0.0025 s, remains constant at 55 C° from 0.0025 s to 0.0075 s, and then decreases from 55 C° to 35 C° between 0.0075 and 0.01.

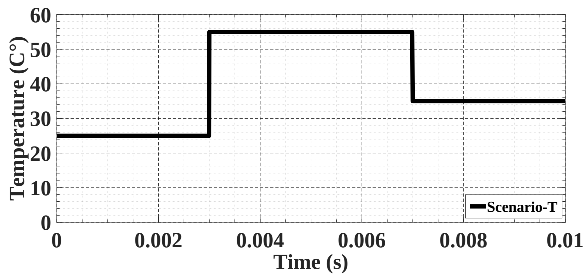


**Fig. 23:** Scenario 3: Temperature variation

Figures 24, 25, and 26 illustrate the evolution of the current, voltage, and power respectively of the PV emulator under temperature variations, controlled by the three strategies (MFC, PI, and FLC) and compared with the reference SW85 PV module.The behavior of the emulator closely matched the predictions made by the electrical model when subjected to temperature changes. This supports the effectiveness of the proposed ANFIS-based PVE design, which employs the MFC Controller, compared with the conventional PI and fuzzy logic FLC controllers. The results indicate that the MFC controller outperforms the other controllers in terms of the overall performance.

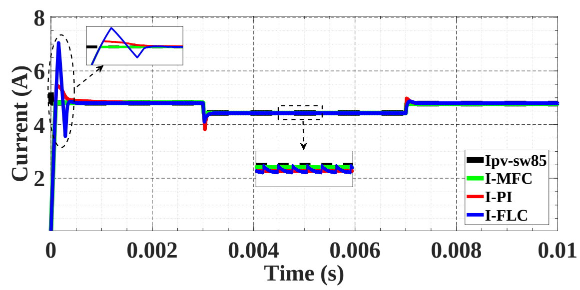


**Fig. 24:** PV emulator current response under temperature variation.

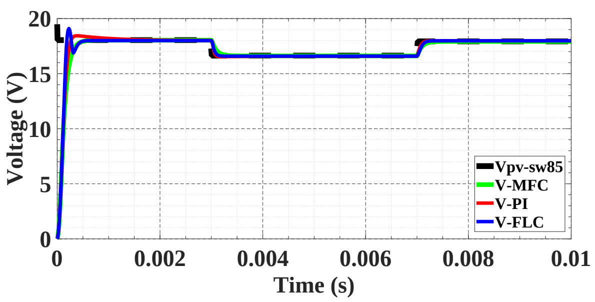


**Fig. 25:** PV emulator voltage response under temperature variation.

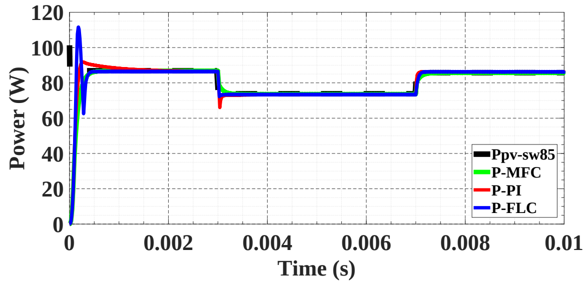


**Fig. 26:** PV emulator power response under temperature variation.

### 3.4. Scenario 4

In this scenario, the proposed PV emulator was tested against the electrical PV panel model during load variations (ramp), covering all load points from short-circuit $(I_{sc}, 0)$ to open-circuit $(0, V_{oc})$ conditions.

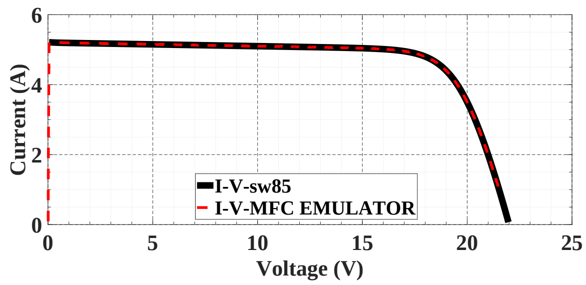


**Fig. 27:** Comparison of I-V characteristics between the real PV panel and the I-V emulator at STC

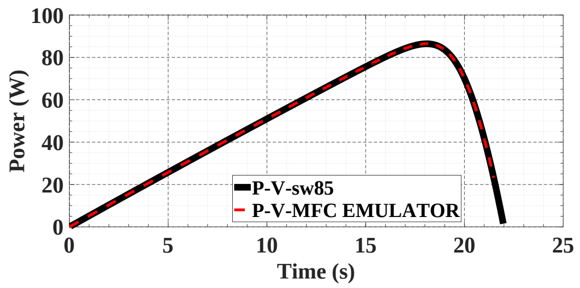


**Fig. 28:** Comparison of P-V characteristics between the real PV panel and the P-V emulator at STC

Figures 27 and 28 illustrates that the performance results effectively reflect the characteristics of the emulator. The I-V and P-V curves were closely aligned with those of the actual electrical model of the PV panel under Standard Test Conditions (STC). This confirms the effectiveness of the proposed emulator. As in the previous scenarios, presents the results, which highlight the reliability of the proposed emulator that integrates the MFC with the ANFIS.

This combination demonstrated its ability to achieve precise tracking and stable performance under various loading conditions. This reliability is essential for validating its applicability in real-world scenarios.

Additionally,Table 8 offers a comparative performance analysis of several photovoltaic emulators, enabling an objective evaluation of the proposed system.

**Tab. 8:** Comparison of the performance of different photovoltaic emulators.

| Authors (Ref) | Converter type | Control complexity | Settling time (ms) | IAE |
|---|---|---|---|---|
| Razman Ayop, [7] | Buck | High complexity | 2.2 | NR |
| Ayop, Razman and Tan, Chee Wei, [37] | Buck | High complexity | 21.25 | NR |
| Esfandiari et al, [9] | Buck | High complexity | 1.5 | 0.0113 |
| Proposed PVE | Buck | High complexity | 0.14 | 2.6056e−04 |

*Note:* NR = Not Rated.

# 4. Conclusion:

This study presented the design and evaluation of a photovoltaic (PV) emulator that integrates an ANFIS-based PV model with a DC–DC buck converter and three control strategies: PI, Fuzzy Logic Control (FLC), and Model-Free Control (MFC). The ANFIS model successfully reproduced the nonlinear I–V and P–V characteristics of PV modules under varying environmental conditions, which enables accurate emulation of PV behavior.

Comparative analysis showed that the MFC strategy provides superior tracking accuracy, faster dynamic response, and improved robustness compared with PI and FLC controllers. These results demonstrate that the proposed ANFIS–MFC framework offers an effective approach for high-fidelity PV emulation.

From a practical perspective, the proposed emulator provides a flexible and cost-effective platform for laboratory testing of photovoltaic energy systems. It can be used to validate Maximum Power Point Tracking (MPPT) algorithms, evaluate DC–DC converter control strategies, and test grid-connected PV systems under controlled and repeatable operating conditions without relying on physical PV panels.

Future work will focus on the hardware implementation of the proposed emulator to enable real-time experimental validation. In addition, more complex environmental conditions, such as partial shading, will be investigated, and the emulator will be further extended to support bifacial PV panels.

## Author Contributions

A.C.: Conceptualization, Methodology, Software, ANFIS Implementation, Writing (Original Draft). A.H.: Supervision, Project Administration, Control Design, Writing (Review & Editing). K.A.: Buck Converter Design, Power Electronics, Hardware, State-Space Analysis. N.A.: Fuzzy Logic & ANFIS Design, Control Strategy Development. M.B.: Model-Free Control, Advanced Algorithms, Performance Analysis. A.R.: Mathematical Modeling, Theoretical Framework, Methodology Oversight.

## Funding

This research received no external funding.

## References

[1] SAYED, E. T., A. G. OLABI, A. H. ALAMI, A. RADWAN, A. MDALLAL, A. REZK and M. A. ABDELKAREEM. Renewable energy and energy storage systems. *Energies*. 2023, vol. 16, iss. 3, pp. 1415. ISSN 1996-1073. DOI: 10.3390/en16031415.

[2] NAGARAJA, M. R., W. K. BISWAS, and C. P. SELVAN. Advancements and challenges in solar photovoltaic technologies: enhancing technical performance for sustainable clean energy – A review. *Solar Energy Advances*, 2024, vol. 5, pp. 100084. ISSN 2667-1131. DOI: 10.1016/j.seja.2024.100084.

[3] AL-ALI, S., OLABI, A. G. and MAHMOUD, M. A review of solar photovoltaic technologies: developments, challenges, and future perspectives. *Energy Conversion and Management: X*. 2025, pp. 101057. DOI: 10.1016/j.ecmx.2025.101057.

[4] OLAYIWOLA, T. N., HYUN, S.-H. and CHOI, S.-J. Photovoltaic modeling: a comprehensive analysis of the I–V characteristic curve. *Sustainability*. 2024, vol. 16, no. 1, pp. 432. DOI: 10.3390/su16010432.

[5] ALOMBAH, N. H., A. HARRISON, S. KAMEL, H. B. FOTSIN and M. AURANGZEB. Development of an efficient and rapid computational solar photovoltaic emulator utilizing an explicit PV model. *Solar Energy*. 2024, vol. 271, pp. 112426. ISSN 0038-092X. DOI: 10.1016/j.solener.2024.112426.

[6] ALAAS, Z. Robust and fast emulation of PV panels using FSL algorithm and nonlinear power stage controller. *Computers and Electrical Engineering*. 2024, vol. 119, pp. 109576. ISSN 0045-7906. DOI: 10.1016/j.compeleceng.2024.109576.

[7] MBARKI, B., F. FETHI, J. CHROUTA and A. ZAAFÖURI. Adaptive neuro-fuzzy inference system algorithm-based robust terminal sliding mode control MPPT for a photovoltaic system. *Transactions of the Institute of Measurement and Control*, 2024, vol. 46, no. 2, pp. 316-325. Sage Publications, UK.DOI: 10.1177/01423312231173022.

[8] CHOI, S., S. PARK, J. HONG and J. WON. A design and validation of 400 W PV emulator using simple equivalent circuit for PV power system test. *Energies*. 2023, vol. 16, iss. 4, pp. 1561. ISSN 1996-1073. DOI: 10.3390/en16041561.

[9] AYOP, R. and C. W. TAN. A comprehensive review on photovoltaic emulator. *Renewable and Sustainable Energy Reviews*. 2017, vol. 80, pp. 430–452. ISSN 1364-0321. DOI: 10.1016/j.rser.2017.05.217.

[10] ESFANDIARI, S., M. DAVARI, W. GAO, Y. YANG and K. AL-HADDAD. A novel converter-based PV emulator control using Lambert W method and fractional-order fuzzy proportional-integral controller trained by Harris Hawks optimization for PV inverter-based resources. *IEEE Journal of Emerging and Selected Topics in Industrial Electronics*. 2024, vol. 5, iss. 4, pp. 1493–1507. ISSN 2687-9735. DOI: 10.1109/JESTIE.2024.3402345.

[11] CHAKER, M., A. EL HOURE, D. YOUSFI, M. KOURCHI, M. AJAAMOUM, H. IDADOUB, and J. BOUCHNAIF. Development of a PV emulator using SMPS converter and a model selection mechanism for characteristic generation. *Solar Energy*, 2022, vol. 239, pp. 117–128. ISSN 0038-092X. DOI: 10.1016/j.solener.2022.04.049.

[12] CHIN,V.J., Z. SALAM and K. ISHAQUE. Cell modelling and model parameters estimation techniques for photovoltaic simulator application: A review. *Applied Energy*. 2015, vol. 154, pp. 500–519. Elsevier. DOI: 10.1016/j.apenergy.2015.05.035.

[13] RAM, J. P., H. MANGHANI, D. S. PILLAI, T. S. BABU, M. MIYATAKE and N. RAJASEKAR. Analysis on solar PV emulators: A review. *Renewable and Sustainable Energy Reviews*. 2018, vol. 81, pp. 149–160. ISSN 1364-0321. DOI: 10.1016/j.rser.2017.07.039.

[14] SAMOSIR, A.S., H. GUSMEDI, A.F. HUDA. Design and implementation of PV emulator based on synchronous buck converter using Arduino Nano microcontroller. *International Journal of Power Electronics and Drive Systems (IJPEDS)*. 2025, vol. 16, no. 1, pp. 448–456. DOI: 10.11591/ijpeds.v16.i1.pp448-456.

[15] TOLEDO, F. J., V. GALIANO, V. HERRANZ and J. M. BLANES. Efficient computation of the photovoltaic single-diode model curve by means of a piecewise linear self-adaptive representation. *Journal of Computational Science*. 2024, vol. 75, pp. 102199. ISSN 1877-7503.DOI: 10.1016/j.jocs.2023.102199.

[16] GHADAMI, N., M. GHEIBI, Z. KIAN, M. G. FARAMARZ, R. NAGHEDI, M. EFTEKHARI, A. M. FATHOLLAHI-FARD, M. A. DULEBENETS and G. TIAN. Implementation of solar energy in smart cities using an integration of artificial neural network, photovoltaic system and classical Delphi methods. *Sustainable Cities and Society*. 2021, vol. 74, pp. 103149. ISSN 2210-6707. DOI: 10.1016/j.scs.2021.103149.

[17] HADJAISSA, A., M. BENMILOUD, K. AMEUR, H. BOUCHNAK and M. DIMEH. Advanced Photovoltaic Emulator with ANN-Based Modeling Using a DC-DC Push-Pull Converter and LQR Control with Current Observer. *Iranian Journal of Electrical & Electronic Engineering*. 2024, vol. 20, iss. 4. ISSN 1735-2827.DOI: 10.22068/IJEEE.20.4.3402.

[18] KHAWALDEH, H.A., M. AL-SOEIDAT, D.D.-C. LU, and L. LI. Accurate, fast and power efficient PV emulator based on hybrid passive and active circuits. *CPSS Transactions on Power Electronics and Applications*, 2022, vol. 7, no. 4, pp. 432–441. DOI: 10.24295/CPSSTPEA.2022.00039.

[19] SHARMA, S. and D. JOSHI et al. Modeling and control of PV emulator with different controllers and transient load conditions. *Indian Journal of Engineering and Materials Sciences*. 2023, vol. 30, iss. 1, pp. 73–79. ISSN 0975-1017.

[20] SHAH, P. and S. AGASHE. Review of fractional PID controller. *Mechatronics*. 2016, vol. 38, pp. 29–41. ISSN 0957-4158. DOI: 10.1016/j.mechatronics.2016.06.005.

[21] MENSIA, N., M. TALBI, and M. BOUAÏCHA. New Adaptive PI Controller for Photovoltaic Systems. *Iranian Journal of Science and Technology, Transactions of Electrical Engineering*, 2024, vol. 48, no. 3, pp. 1099–1110. DOI: 10.1007/s40998-024-00734-w.

[22] BOUDIA, A., S. MESSALTI, S. ZEGHLACHE, and A. HARRAG. Type-2 fuzzy logic controller-based maximum power point tracking for photovoltaic system. *Electrical Engineering & Electromechanics*, 2025, no. 1, pp. 16–22. DOI: 10.20998/2074-272X.2025.1.03.

[23] FATHI, M. and J. A. PARIAN. Intelligent MPPT for photovoltaic panels using a novel fuzzy logic and artificial neural networks based on evolutionary algorithms. *Energy Reports*. 2021, vol. 7, pp. 1338–1348. Elsevier. DOI: 10.1016/j.egyr.2021.02.051.

[24] AYOP, R., C. W. TAN, S. M. AYOB, N. D. MUHAMAD, J. J. JAMIAN, and Z. A. NOORDEN. Photovoltaic emulator using error adjustment fuzzy logic proportional-integral controller. *Int. J. Power Electr. Drive Syst. (IJPEDS)*, vol. 13, no. 2, 2022, pp. 1111–1118. DOI: 10.11591/ijpeds.v13.i2.21150.

[25] MOSTAFA, M. R., N. H. SAAD and A. A. EL-SATTAR. Tracking the maximum power point of PV array by sliding mode control method. *Ain Shams Engineering Journal*. 2020, vol. 11, iss. 1, pp. 119–131. DOI: 10.1016/j.asej.2019.09.003.

[26] BOUBAKIR, A., S. A. TOUIL, S. LABIOD, and N. BOUDJERDA. A robust model-free controller for a three-phase grid-connected photovoltaic system based on ultra-local model. *Protection and Control of Modern Power Systems*, vol. 6, no. 1, 2021, p. 43. DOI: 10.1186/s41601-021-00218-7.

[27] ZHAO, Y., A. AN, Y. XU, Q. WANG and M. WANG. Model predictive control of grid-connected PV power generation system considering optimal MPPT control of PV modules. *Protection and Control of Modern Power Systems*. 2021, vol. 6, iss. 1, pp. 32. ISSN 2367-2617. DOI: 10.1186/s41601-021-00210-1.

[28] SEGUEL, J. L., S. I. SELEME JR and L. M. F. MORAIS. Comparative study of Buck-Boost, SEPIC, Cuk and Zeta DC-DC converters using different MPPT methods for photovoltaic applications. *Energies*. 2022, vol. 15, iss. 21, pp. 7936. ISSN 1996-1073. DOI: 10.3390/en15217936.

[29] MUMTAZ, F., N. Z. YAHAYA, S. T. MERAJ, B. SINGH, R. KANNAN and O. IBRAHIM. Review on non-isolated DC-DC converters and their control techniques for renewable energy applications. *Ain Shams Engineering Journal*. 2021, vol. 12, iss. 4, pp. 3747–3763. DOI: 10.1016/j.asej.2021.03.022.

[30] ZHU, W., A. HARRISON, J. DE DIEU NGUIMFACK-NDONGMO, S. IQBAL, N. H.

ALOMBAH, W. F. MBASSO, H. A. MAHMOUD and B. N. ALHASNAWI. A novel simplified buck power system control algorithm: Application to the emulation of photovoltaic solar panels. *Computers and Electrical Engineering*. 2024, vol. 116, pp. 109161. ISSN 0045-7906. DOI: 10.1016/j.compeleceng.2024.109161.

[31] GAHGOUHI, S., A. HADJAISSA, K. AMEUR, A. RABHI and M. KIOUS. A novel Fuzzy-PI-based control for PEM fuel cell emulator based on a buck converter. *Energy Systems*. 2024, pp. 1–20. ISSN 1868-3967. DOI: 10.1007/s12667-024-00680-w.

[32] HARRISON, A., N. H. ALOMBAH, S. KAMEL, S. S. M. GHONEIM, I. EL MYASSE and H. KOTB. Towards a simple and efficient implementation of solar photovoltaic emulator: An explicit PV model based approach. *Engineering Proceedings*. 2023, vol. 56, iss. 1, art. 261. DOI: 10.3390/ASEC2023-16268.

[33] IDRISSI, Y. E. A., K. ASSALAOU, L. ELMAHNI and E. AITIAZ. New improved MPPT based on artificial neural network and PI controller for photovoltaic applications. *International Journal of Power Electronics and Drive Systems*. 2022, vol. 13, iss. 3, pp. 1791–1801. ISSN 2088-8694. DOI: 10.11591/ijpeds.v13.i3.pp1791-1801.

[34] YILMAZ, U., A. KIRÇAY and S. BOREKCI. PV system fuzzy logic MPPT method and PI control as a charge controller. *Renewable and Sustainable Energy Reviews*. 2018, vol. 81, pp. 994–1001. DOI: 10.1016/j.rser.2017.08.048.

[35] AYOP, R. and C. W. TAN. Rapid prototyping of photovoltaic emulator using buck converter based on fast convergence resistance feedback method. *IEEE Transactions on Power Electronics*. 2019, vol. 34, no. 9, pp. 8715–8723. DOI: 10.1109/TPEL.2018.2886927.

[36] DÍAZ-RODRÍGUEZ, I. D., S. HAN, L.H. KEEL and S.P. BHATTACHARYYA. Advanced tuning for Ziegler-Nichols plants. *IFAC-PapersOnLine*. 2017, vol. 50, iss. 1, pp. 1805–1810. DOI: 10.1016/j.ifacol.2017.08.168.

[37] CHANDRASEKARAN, S., S. DURAIRAJ and S. PADMAVATHI. A performance evaluation of a fuzzy logic controller-based photovoltaic-fed multi-level inverter for a three-phase induction motor.*Journal of the Franklin Institute*. 2021, vol. 358, no. 15, pp. 7394–7412. DOI: 10.1016/j.jfranklin.2021.07.032.

[38] SENG, U. K., H. MALIK, F. P. G. MÁRQUEZ, M. A. ALOTAIBI and A. AFTHANORHAN. Fuzzy logic-based intelligent energy management framework for hybrid PV-wind-battery system: A case study of commercial building in Malaysia. *Journal of Energy Storage*. 2024, vol. 102, pp. 114109. ISSN 2352-152X. DOI: 10.1016/j.est.2024.114109.

[39] FLIESS, M. and C. JOIN. Model-free control. *International journal of control*. 2013, vol. 86, iss. 12, pp. 2228–2252. ISSN 0020-7179. DOI: 10.1080/00207179.2013.810345.

[40] FLIESS, M. Model-free control and intelligent PID controllers: towards a possible trivialization of nonlinear control *IFAC Proceedings Volumes*. 2009, vol. 42, iss. 10, pp. 1531–1550. ISSN 1474-6670. DOI: 10.3182/20090706-3-FR-2004.00256.

[41] MOUSSA, I., A. KHEDHER and A. BOUALLEGUE. Design of a low-cost PV emulator applied for PVECS. *Electronics*. 2019, vol. 8, iss. 2, pp. 232. ISSN 2079-9292. DOI: 10.3390/electronics8020232.

[42] GUERRA, M. I. S., F. M. U. DE ARAÚJO, J. T. DE CARVALHO NETO and R. G. VIEIRA. Survey on adaptative neural fuzzy inference system (ANFIS) architecture applied to photovoltaic systems. *Energy Systems*. 2024, vol. 15, no. 2, pp. 505–541. DOI: 10.1007/s12667-022-00513-8.

[43] ALI, O. F., R. A. FAYADH, M. J. MNATI and T. S. EL-HASAN. Enhanced efficiency of a photovoltaic system by the implementation of an adaptive neuro-fuzzy inference system (ANFIS) using MATLAB/SIMULINK to extract maximum powerpoint (MPP). In:*AIP Conference Proceedings*, vol. 3232, no. 1, 2024, pp. 050010. DOI: 10.1063/5.0236364.

[44] BABES, B., S. LATRÈCHE, A. BOUAFASSA, O. AISSA, A. E. BADOUD, M. KHEMLICHE, M. BAJAJ and I. ZAITSEV. A dSPACE-based implementation of ANFIS and predictive current control for a single phase boost power factor corrector. *Scientific Reports*. 2024, vol. 14, no. 1, p. 12775. DOI: 10.1038/s41598-024-63740-2.

[45] TORCHANI, B., A. TAHER AZAR , A. SELLAMI, S. AHMED, I.A. HAMEED, I.KASIM IBRAHEEM and M.I.J. AL-OBAIDI. Adaptive sliding mode control based on maximum power point tracking for boost converter of photovoltaic system under reference voltage optimizer. *Frontiers in Energy Research*. 2024, vol. 12, pp. 1485470. DOI: 10.3389/fenrg.2024.1485470.